Volume 24, No 4 | International Journal of Radiation Research, October 2026

Research on the application of multi-parametric MRI radiomics based on different regions of interest in the evaluation of benign and malignant prostate lesions

W. Zhao, L. Zhang*, L. Wang, L. Chen, D. Li

Department of Radiology, Huaibei People's Hospital, Huaibei, Anhui, China

► ***Original article***

Corresponding author:
Lei Zhang, M.D.,
E-mail: *452473418@qq.com*

Received: April 2025
Final revised: November 2025
Accepted: January 2026

Int. J. Radiat. Res., October 2026; 24(4): 1181-1187

DOI: 10.61186/ijrr.24.4.32

Keywords: *Prostate cancer, radiomics, machine learning, multiparametric magnetic resonance imaging.*

ABSTRACT

Background: The aim was to examine the diagnostic utility of radiomics via multi-parametric magnetic resonance imaging (mpMRI) in distinguishing between benign and malignant prostate lesions when features are extracted from different regions of interest (ROIs). ***Materials and Methods:*** A retrospective cohort of 99 individuals having mpMRI (T2WI, DCE, ADC) with histopathological confirmation was analyzed and split into training (n = 69) and validation (n = 30) at random as 7:3. Radiomics characteristics were taken from two ROIs: the lesion area (Set 1) and the whole-prostate area (Set 2). After choice of features by least absolute shrinkage and selection operator (LASSO), logistic regression (LR) was utilized to generate three models: Model 1 (lesion-based radiomics), Model 2 (prostate-based radiomics), and Model 3 (combined radiomics plus clinical factors). Receiver operating characteristic (ROC) was utilized to evaluate diagnostic results, and inter-model comparisons were conducted with DeLong's test. ***Results:*** Of the 99 patients, 59 had benign and 40 had malignant lesions. In the training set, the area under the curve (AUC) values of Models 1, 2, and 3 were 0.997 (0.991–1.000), 0.969 (0.937–1.000), and 0.999 (0.997–1.000), while the corresponding validation AUCs were 0.920 (0.829–1.000), 0.916 (0.820–1.000), and 0.929 (0.843–1.000). There were no statistically significant variations among the three models. ***Conclusion:*** Radiomics models derived from mpMRI, regardless of whether features are extracted from the lesion area or from the entire prostate, demonstrate strong diagnostic capability in differentiating between prostate tumors that are benign and cancerous, suggesting substantial potential for clinical application.

INTRODUCTION

The 2nd most frequent cancer and one of the main causes of cancer-related death for men globally is prostate cancer (PCa). In Asia, the disease burden continues to rise rapidly, with diagnoses frequently occurring at advanced stages and associated with poorer outcomes [1]. Although prostate-specific antigen (PSA) testing remains commonly employed, its limited specificity often results in overdiagnosis and unnecessary biopsies, imposing substantial physical and psychological burdens on patients [2]. mpMRI, integrating T2WI, DCE imaging, and ADC maps - has become the reference standard for prostate imaging and risk stratification [3]. T2WI provides detailed anatomical delineation, where suspicious peripheral-zone lesions typically appear as regions of low signal intensity [4]. Diffusion-weighted imaging (DWI)-derived ADC maps capture water diffusivity; diffusion restriction caused by increased cellular density in malignant lesions significantly enhances tumor conspicuity [5, 6]. Although the Prostate Imaging Reporting and Data System version 2.1 (PI-RADS v2.1) has improved the identification of clinically significant PCa (csPCa) [7], challenges remain. PI-RADS 3 lesions continue to present diagnostic uncertainty, with csPCa detection rates ranging from 12.5% to 20.8% [8], and up to 40% of csPCa may remain occult on mpMRI due to small lesion size or low Gleason components [9]. These limitations underscore the need for complementary diagnostic tools.

Radiomics has become a promising method for extracting high-dimensional quantitative features from medical images in prostate cancer precision diagnostics [10]. Previous studies demonstrate the use of radiomics based on mpMRI to distinguish between benign and malignant lesions and in predicting clinically relevant pathological outcomes [11]. However, several important gaps remain. Most existing radiomics models rely predominantly on lesion-based regions of interest (ROIs), potentially overlooking diffuse or subtle pathological changes that may be captured when using whole-prostate ROIs [12]. Moreover, the optimal integration of multi-sequence mpMRI radiomics features from different ROIs is insufficiently explored, and direct comparative analyses of lesion-based versus prostate-based models are scarce [13]. While a recent 2024 multi-center investigation validated mpMRI radiomics for predicting genomic alterations in PCa, similarly rigorous evaluations for benign–malignant

[Downloaded from ijrr.com on 2026-11-23]

[DOI: 10.61186/ijrr.24.4.32]

differentiation across varying ROI strategies remain limited [14]. The absence of standardized ROI selection hampers clinical translation, particularly for indeterminate PI-RADS 3 lesions or mpMRI-invisible csPCa [15].

We hypothesize that radiomics features extracted from both lesion-specific and whole-prostate ROIs capture complementary biological information and could therefore improve the accuracy of differentiating between benign and cancerous prostate tumors. Accordingly, the primary objective is to assess the diagnostic performance of mpMRI-based radiomics features derived from various ROIs. Specifically, we aim to construct and validate multi-modal radiomics models incorporating T2WI, DCE, and ADC sequences, and to compare their diagnostic efficacy.

This work has important theoretical and clinical implications. Methodologically, it offers new insights into ROI optimization strategies for prostate radiomics. Clinically, the proposed models have the potential to enhance diagnostic specificity, reduce unnecessary biopsies, and facilitate individualized decision-making, especially for mpMRI-challenging lesions. From a broader public health perspective, a reliable non-invasive diagnostic tool could refine early screening strategies, alleviate healthcare system burden, and ultimately improve patient outcomes. Additionally, the multi-sequence radiomics framework established in this study provides a foundation for future large-scale, multi-center validation.

MATERIALS AND METHODS

General information

The Ethics Committee of Huaibei People's Hospital accepted this retrospective work (Approval No. 2024-088), and because of its retrospective nature, informed consent was not required.

A sum of 99 individuals undergoing prostate mpMRI followed by biopsy or postoperative pathological examination at Huaibei People's Hospital were examined in retrospect from January 2020 to April 2024. The following were the requirements for inclusion:

(1) mpMRI performed at our institution; (2) elevated PSA levels; (3) first-time clinical evaluation with a confirmed diagnosis; and (4) complete and accurate clinical and demographic information. Exclusion criteria included:

(1) prior prostate biopsy or surgery before MRI; (2) history of pelvic radiotherapy, chemotherapy, endocrine therapy, or surgery within 6 months before MRI; (3) lesion volume <5 mm^3, precluding reliable ROI delineation; and (4) severe imaging artifacts compromising diagnostic quality or preventing accurate ROI delineation and subsequent analysis.

Equipment and related parameters

All MRI scans were obtained with a Philips Ingenia 3.0-T MR scanner. T2WI, DCE-MRI, and ADC maps made up the mpMRI procedure. Key imaging parameters were as follows:

1. T2WI: TR = 3544 ms, TE = 100 ms, flip angle = 90°, FOV = 240 × 240 mm^2, slice thickness = 3 mm, slice gap = 0.6 mm, matrix = 180 × 159, excitation = 1.
2. DCE-MRI: TR = 4.6 ms, TE = 1.42 ms, flip angle = 90°, FOV = 240 × 240 mm^2, slice thickness = 3 mm, slice gap = 1.5 mm, matrix = 180 × 159, excitation = 2.
3. ADC: ADC maps were generated using a standard single-exponential diffusion model.

Image segmentation

DICOM images were imported into an AI-based radiomics analysis platform (https://www.huiyihuiying.com). A radiologist with eight years of experience performing prostate MRIs (Radiologist A) manually delineated lesion ROIs and whole-prostate ROIs on mpMRI sequences, referencing pathological results as the reference standard. ROIs were drawn as close as possible to the tumor margin while excluding hemorrhage, necrosis, and calcification. When a patient has several lesions, the slice containing the largest lesion with the highest Gleason score was selected. Representative imaging features of benign and malignant prostate lesions on DCE-MRI are shown in figure 1.

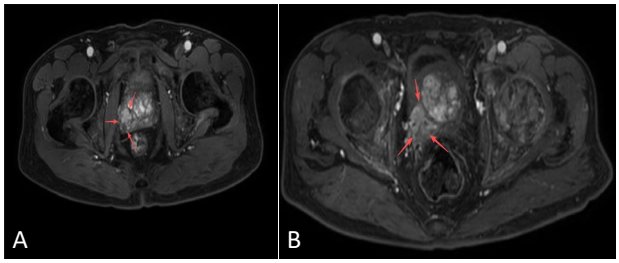


Figure 1. Imaging features of benign and malignant prostate cancer on DCE-MRI. **(A)** benign prostate lesions show mild-to-moderate, homogeneous enhancement with slow signal rise and no obvious washout. **(B)** Malignant lesions exhibit marked, heterogeneous enhancement-rapid early signal elevation followed by rapid washout, distinct from benign and normal prostate tissue.

Feature extraction and screening

The PyRadiomics (version 3.1.0) library in Python 3.6.8 was used to extract characteristics from radiomics. Each image set yielded a total about 1688 quantitative radiomics characteristics. Thirty patients were chosen at random to evaluate repeatability both within and between observers. Radiologist A and Radiologist B independently redelineated ROIs after a two-week period. The value of the intra-class correlation coefficient (ICC) > 0.80 indicates good feature stability. Z-score normalization was used to normalize all features. In order to reduce dimensionality and choose features, LASSO regression was utilized. The best regularization parameter (λ) was found via ten-fold cross validation. Based on the chosen features and their coefficients, a

[Downloaded from ijrr.com on 2026-11-23]

[DOI: 10.61186/ijrr.24.4.32]

radiomics score (Radscore) was then computed for every patient.

Radiomics model construction and evaluation

LR classifiers were employed in the construction of three diagnostic models:

1. Model 1: Multi-sequence radiomics features from lesion-based ROIs
2. Model 2: Multi-sequence radiomics features from whole-prostate ROIs
3. Model 3: Combined model integrating optimal radiomics features with clinical variables (age and PSA)

The area under ROC, sensitivity, specificity, accuracy, and F1-score were utilized to assess the model's performance. AUCs were compared between models via DeLong test. Calibration curves and the Hosmer-Lemeshow goodness-of-fit test were used to assess calibration. DCA was used to assess clinical utility.

Statistical analysis

The Shapiro-Wilk test was used to determine whether continuous variables were normal. The median (interquartile range) was used to display non -normally distributed data, whereas the mean ± standard deviation was used to express scattered data. Independent-sample t-tests were utilized on variables that had a normal distribution. Meanwhile, Mann-Whitney U test for variables with non-normal distributions. Statistical significance was defined as a two-sided p-value of less than 0.05.

RESULTS

Basic information

This work had 99 patients in total. The average age was 70.9 ± 9.3 years, and the mean PSA level was 34.1 ± 36.0 ng/mL. Among them, 59 cases were diagnosed as benign and 40 as malignant. Statistical analyses revealed significant disparities in age and PSA levels between two groups ($p<0.05$). Table 1 summarizes specific clinical and demographic traits. The training set (n = 69) and the validation set (n = 30) were randomly assigned to each patient as 7:3.

Table 1. General information of the two groups of subjects.

	Benign (n=59)	Malignant (n=40)	p-value
Age	69.2±9.0	73.5±9.1	0.012
PSA (ng / ml)	22.2±20.0	51.5±45.9	0.004

Feature screening

T2WI, ADC, and DCE images were used to extract 1,688 radiomics characteristics for both lesion-based and prostate-based ROIs. After reproducibility analysis using ICC and dimensionality reduction via LASSO, there were 29 features kept for the lesion-based ROI and 18 for the prostate-based ROI. LASSO selection results are displayed in figure 2, where the left panel shows the mean square error plot and the right panel illustrates the coefficient profiles. In the figure, "A" denotes the lesion-based features and "B" the prostate-based features. The corresponding feature coefficients are provided in figure 3.

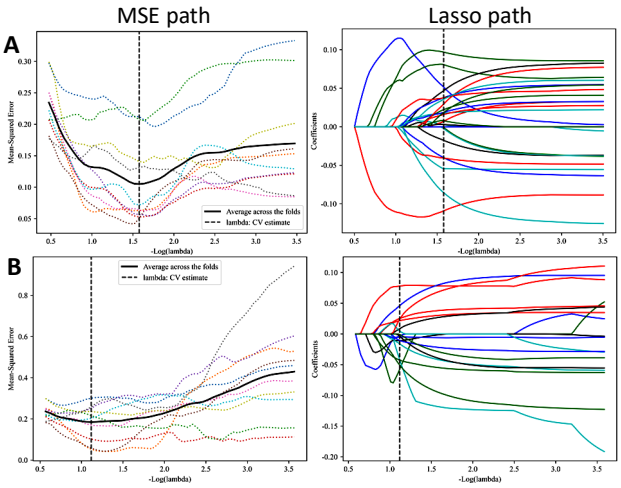


Figure 2. Path diagram of LASSO algorithm screening for multi-sequence omics feature domains based on lesion areas and imaging features of the prostate region, as well as the retained best features. **(A)** represents the lesion area, and **(B)** represents the prostate region. The left graph is the mean square error graph, and the right graph is the regression feature coefficient gra.

Model Establishment and evaluation

LR classifiers were used to construct three predictive models:

1. Model 1: lesion-based multi-sequence radiomics model
2. Model 2: prostate-based multi-sequence radiomics model
3. Model 3: combined model incorporating selected radiomics features with clinical factors (age and PSA)

Model performance metrics for both training and validation sets were summarized in table 2. In training, AUCs of models 1, 2, and 3 were 0.997, 0.969, and 0.999. In validation, AUCs were 0.920, 0.916, and 0.929. Across both cohorts, accuracy, specificity, sensitivity, precision, and F1-scores indicated strong predictive performance for all models. The three models' AUCs did not differ statistically significantly, according to the DeLong test ($p>0.05$), suggesting comparable discriminatory power.

Figure 4 displays the three models' ROC curves, with the left and right panels corresponding to training and validation sets. For model 3, the visual nomogram, calibration curve, and DCA are presented in figures 5a-5c, respectively. The calibration curves (figure 5b) demonstrate favorable agreement between predicted probabilities and pathological findings in both cohorts. Similarly, the decision curves (figure 5c) show that the combined method has a significant net therapeutic advantage via a wide variety of threshold probabilities.

[Downloaded from ijrr.com on 2026-11-23]

[DOI: 10.61186/ijrr.24.4.32]

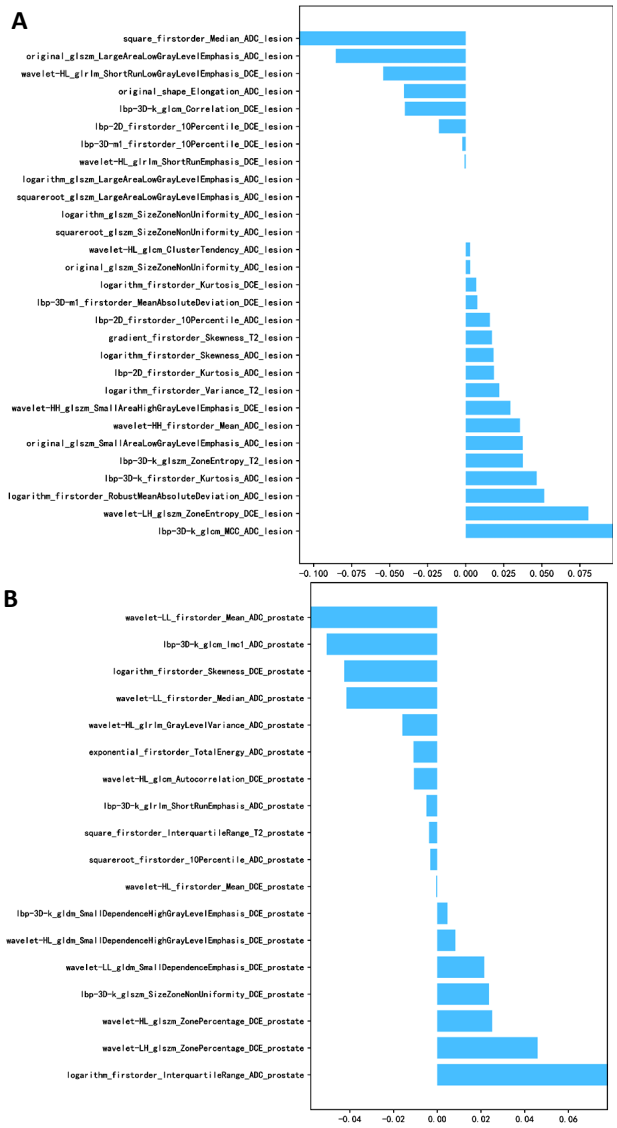


Figure 3. Imaging omics feature and coefficient graph. **(A)** represents the lesion area, and **(B)** represents the prostate region.

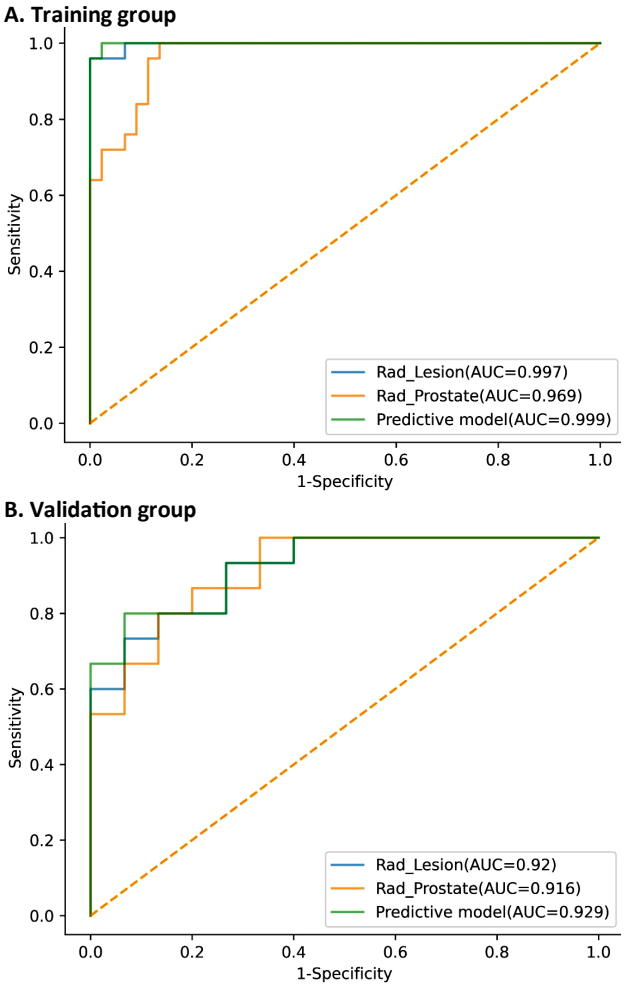


Figure 4. ROC curves of the three models. **(A)** graph is for the training group, and **(B)** graph is for the validation group.

[Downloaded from ijrr.com on 2026-11-23]

[DOI: 10.61186/ijrr.24.4.32]

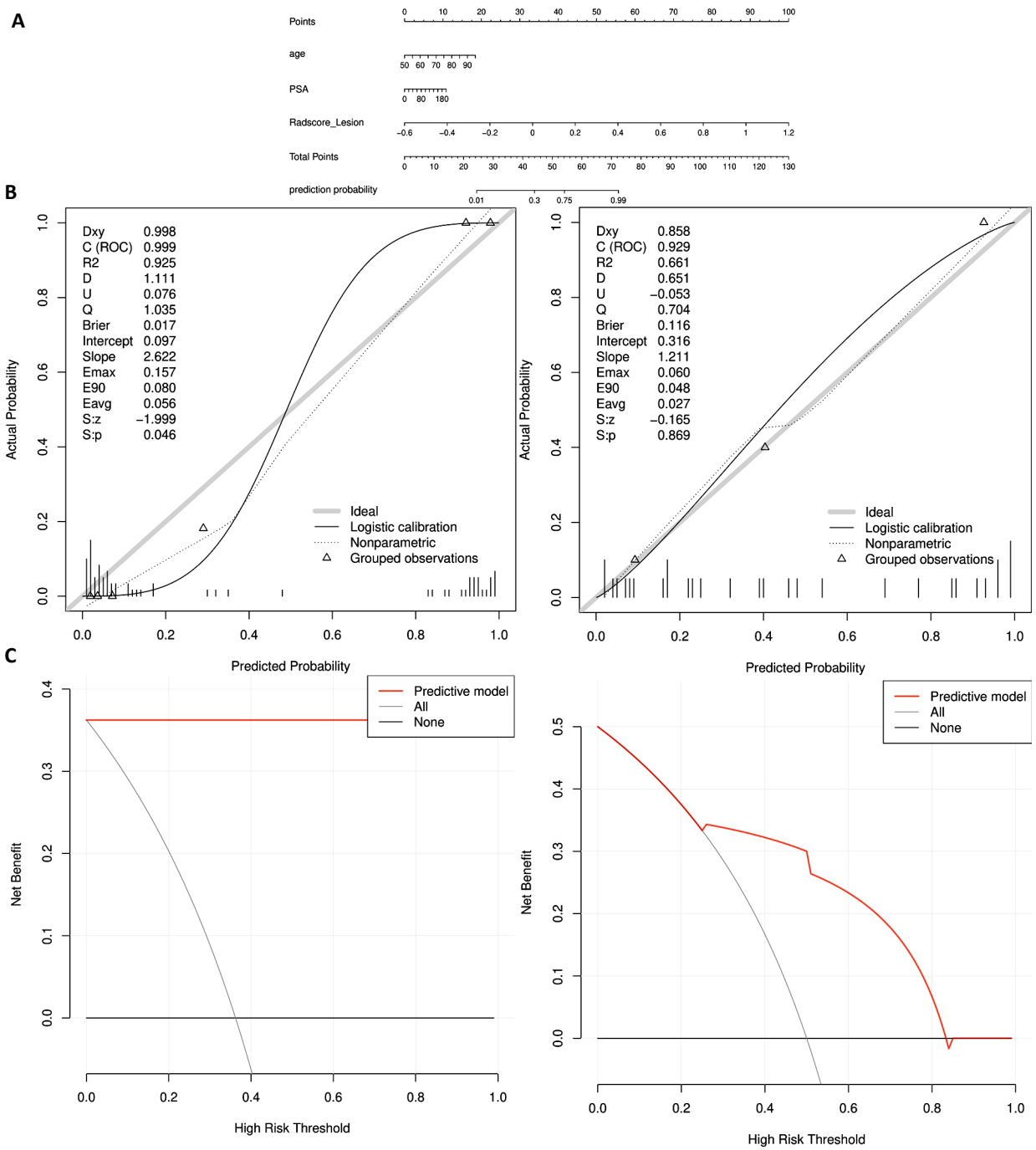


Figure 5. Evaluation of the combined model results. **(A)** Visual nomogram of the combined model; **(B)** Calibration curve of the combined model; **(C)** Decision curve of the combined model. The left graph is for the training group, and the right graph is for the validation group.

DISCUSSION

In this work, we created and verified LR, based radiomics models using features extracted from lesion-level and whole-prostate–level regions on T2WI, DCE, and ADC sequences. Our results demonstrated that the model integrating clinical variables with lesion-derived radiomics features overpass other methods, although no statistically significant differences were observed among the three models.

MpMRI became the method of choice for local PCa assessment imaging, as it offers reliable information regarding tumor localization and extent [16]. Consistent with [17], which reported that combining high b-value DWI and T2WI enhances the sensitivity of PCa detection, our lesion-based and prostate-based models both yielded high AUCs in the test cohort. These results indicate that both ROI strategies can capture discriminative radiological signatures associated with PCa, supporting their value in early disease identification and clinical decision-making. Nevertheless, prior research has indicated that mpMRI alone may be insufficient for accurately evaluating locally advanced PCa and shouldn't be relied upon as the sole tool for

[Downloaded from ijrr.com on 2026-11-23]
[DOI: 10.61186/ijrr.24.4.32]

preoperative staging [18]. This limitation may stem from the expertise required for accurate lesion delineation, the susceptibility of manual segmentation to inter-observer variability, and the reduced sensitivity of lesion-centered approaches for small or early-stage lesions. Starobinets *et al.* [19] further reported that while mpMRI struggles to differentiate sparse from dense lesions, it remains effective for distinguishing malignant lesions from benign tissues.

In our analysis, the prostate-based method obtained AUCs of 0.969 (training) and 0.916 (test), underscoring its potential for capturing global prostate characteristics. This whole-gland approach may facilitate the detection of multifocal or small, inconspicuous lesions and provide clinicians with a more comprehensive understanding of the overall disease burden. However, including normal prostate tissue inevitably introduces additional biological variability- stemming from factors such as prostate size, anatomical heterogeneity, and patient age- which may affect diagnostic stability and reduce sensitivity for early lesions [20, 21]. Recent studies have attempted to address these challenges by integrating multimodal data and advanced modeling strategies. For instance, Zhang *et al.* [22] employed a multimodal extract–transform–load pipeline in 4747 patients across nine institutions and developed the AutoML-based PCAIDS model, which achieved 95% sensitivity for clinically significant PCa (csPCa) and reduced unnecessary biopsies by 32.2% – 36.3%. Another multicenter retrospective study [23] showed that APT-weighted MRI combined with serum PSA effectively differentiates malignant from benign lesions. In addition, [24] created a nomogram that combined age, PI-RADS v2.1, and radiomics scores, demonstrating strong calibration and clinical utility in predicting PCa and reducing unnecessary biopsies among patients with gray-zone PSA. Building on these findings, our combined model incorporated lesion-specific radiomics features along with key clinical indicators (age and PSA), aiming to better reflect both tumor biology and patient status. This strategy led to further performance improvements, with AUCs of 0.999 (training) and 0.929 (testing). Although the DeLong test did not find notable variations between the three types, the combined model showed enhanced robustness and accuracy, highlighting the clinical benefit of integrating imaging with clinical data.

Despite its promising results, this study has a number of shortcomings:

The study is conducted at a single center with a relatively small sample size, and external validation across diverse institutions is needed to confirm generalizability.

Automated ROI segmentation methods remain immature, and reliance on manual segmentation increases workload and inter-observer variability, potentially affecting model reproducibility.

Certain clinically relevant variables, such as tumor volume, were not included as covariates, which may have limited the model's predictive capacity.

In conclusion, mpMRI-based multimodal radiomics models demonstrate substantial clinical value when distinguishing between benign and cancerous prostate tumors. These models provide important decision-support tools for prostate illness diagnosis and treatment, although further external validation and methodological refinement are warranted.

***Acknowledgments*:** Not applicable.

***Availability of data and materials*:** The data and materials supporting the conclusion is provided upon reasonable request.

***Ethics approval and consent to participate*:** This work was authorized by the Medical Ethics Committee and the requirement for patient consent has waived.

***Fundings*:** This work did not obtain any outside financing.

***Conflict of interest*:** The writers affirm that they have no competing interests.

***Consent for publication*:** Not applicable.

***Author contributions*:** W.Z., Data analysis and writing - first draft. L.Z., Writing - first draft. L.W., Software, writing - reviewing and editing. D.L., Methodology and supervision. L.C., Data collection and images analysis.

REFERENCES

1. Zhou S, Ren H, Zhu K, Cheng S (2025) Performance of PSMA PET-CT imaging in predicting outcomes and assessing response in prostate cancer: a meta-analysis. *Int J Radiat Res,* ***23****(3): 665-675*.
2. Kasivisvanathan V, Rannikko AS, Borghi M, *et al.* (2018) MRI-Targeted or Standard Biopsy for Prostate-Cancer Diagnosis. *N Engl J Med,* ***378****(19): 1767-1777*.
3. Demir F, Karaçavuş S, Gençer H, Özdal A, Erdoğan Z, Çiftçi İ, *et al.* (2025) Relationship between tumor parameters in Ga-68 PSMA PET/CT and pathological grade grouping in patients with prostate cancer. *Int J Radiat Res,* ***23****(2): 277-281*.
4. Teică RV, Șerbănescu MS, Florescu LM, *et al.* (2023) Tumor area highlighting using T2WI, ADC map, and DWI sequence fusion on bpMRI images for better prostate cancer diagnosis. *Life (Basel),* ***13*** *(4): 910*.
5. Thörmer G, Otto J, Reiss-Zimmermann M, *et al.* (2012) Diagnostic value of ADC in patients with prostate cancer: influence of the choice of b values. *Eur Radiol,* ***22****(8): 1820-1828*.
6. Arita Y, Yoshida S, Waseda Y, *et al.* (2021) Diagnostic value of computed high b-value whole-body diffusion-weighted imaging for primary prostate cancer. *Eur J Radiol,* ***137****: 109581*.
7. Wei X, Xu J, Zhong S, *et al.* (2022) Diagnostic value of combining PI-RADS v2.1 with PSAD in clinically significant prostate cancer. *Abdom Radiol (NY),* ***47****(10): 3574-3582*.
8. Sadati E, Hashemi B, Mahdavi S, Nikoufar A, Abdollahi H (2025) Predicting prostate cancer radiotherapy complications: An integrated approach using radiomics, dosiomics, and machine learning. *Int J Radiat Res,* ***23****(1): 239-244*.
9. Wang L, Mazaheri Y, Zhang J, Ishill NM, *et al.* (2008) Assessment of biologic aggressiveness of prostate cancer: correlation of mr signal intensity with Gleason grade after radical prostatectomy. *Radiology,* ***246****(1): 168-176*.

[Downloaded from ijrr.com on 2026-11-23]

[DOI: 10.61186/ijrr.24.4.32]

10. Lambin P, Rios-Velazquez E, Leijenaar R, Carvalho S, *et al.* (2012) Radiomics: extracting more information from medical images using advanced feature analysis. *Eur J Cancer,* ***48****(4): 441-446*.
11. Stoyanova R, Takhar M, Tschudi Y, *et al.* (2016) Prostate cancer radiomics and the promise of radiogenomics. *Trans Cancer Res,* ***5*** *(4): 432-447*.
12. Murakami Y, Soyano T, Kozuka T, *et al.* (2022) Dose-based radiomic analysis (dosiomics) for intensity modulated radiation therapy in patients with prostate cancer: correlation between planned dose distribution and biochemical failure. *Int J Radiat Oncol Biol Phys,* ***112****(1): 247-259*.
13. Zhang H, Li XL, Zhang YX, *et al.* (2021) Diagnostic nomogram based on intralesional and perilesional radiomics features and clinical factors of clinically significant prostate cancer. *J Magn Reson Imaging,* ***53****(5): 1550-1558*.
14. Woźnicki P, Westhoff N, Huber T, *et al.* (2020) Multiparametric MRI for prostate cancer characterization: combined use of radiomics model with PI-RADS and clinical parameters. *Cancers,* ***12*** *(7): 1767*.
15. Zhang YS, Chen W, Yue XJ, *et al.* (2020) Development of a novel, multi-parametric, MRI-based radiomic nomogram for differentiating between clinically significant and insignificant prostate cancer. *Front Oncol,* ***10****: 888*.
16. Caglic I, Kovac V, Barrett T (2019) Multiparametric MRI-local staging of prostate cancer and beyond. *Radiol Oncol,* ***53****(2): 159-170*.
17. Colvin SD, Cason DE, Galgano SJ, *et al.* (2020) Fusion of high B-value diffusion-weighted and T2-weighted MR images increase sensitivity for identification of extraprostatic disease in prostate cancer. *Clin Imaging,* ***68****: 202-209*.
18. Chandrasekar T, Denisenko A, Mico V, *et al.* (2023) Multiparametric MRI is not sufficient for prostate cancer staging: A single institutional experience validated by a multi-institutional regional collaborative. *Urol Oncol,* ***41****(8): 355. e1-355*.e8.
19. Starobinets O, Simko JP, Gibbons M, *et al.* (2024) The impact of benign tissue within cancerous regions in the prostate: Characterizing sparse and dense prostate cancers on whole-mount histopathology and on multiparametric MRI. *Magn Reson Imaging,* ***114****: 110233*.
20. Scheenen TW, Rosenkrantz AB, Haider MA, *et al.* (2015) Multiparametric magnetic resonance imaging in prostate cancer management: Current status and future perspectives. *Invest Radiol,* ***50****(9): 594-600*.
21. Ito K, Furuta A, Kido A, *et al.* (2020) Detectability of prostate cancer in different parts of the gland with 3-Tesla multiparametric magnetic resonance imaging: correlation with whole-mount histopathology. *Int J Clin Oncol,* ***25****(4): 732-740*.
22. Zhang H, Ji J, Liu Z, *et al.* (2023) Artificial intelligence for the diagnosis of clinically significant prostate cancer based on multimodal data: a multicenter study. *BMC Med,* ***21****(1): 270*.
23. Yang L, Wang L, Tan Y, *et al.* (2023) Amide Proton Transfer-weighted MRI combined with serum prostate-specific antigen levels for differentiating malignant prostate lesions from benign prostate lesions: a retrospective cohort study. *Cancer Imaging,* ***23*** *(1): 3*.
24. Zhang L, Zhang J, Tang M, *et al.* (2022) MRI-based radiomics nomogram for predicting prostate cancer with gray-zone prostate-specific antigen levels to reduce unnecessary biopsies. *Diagnostics (Basel),* ***12****(12): 3005*.

[Downloaded from ijrr.com on 2026-11-23]

[DOI: 10.61186/ijrr.24.4.32]

[DOI: 10.61186/ijrr.24.4.32] [Downloaded from ijrr.com on 2026-11-23]